Inorganic Chemistry

Article

pubs.acs.org/IC

OMS, OM(η^2-SO), and OM(η^2-SO)(η^2-SO_2) Molecules (M = Ti, Zr, Hf): Infrared Spectra and Density Functional Calculations

Xing Liu,[†] Xuefeng Wang,*[,†] Qiang Wang,[†] and Lester Andrews*[,‡]

[†]Department of Chemistry, Tongji University, Shanghai, 200092, China

[‡]Department of Chemistry, University of Virginia, Charlottesville, Virginia 22904, United States

ABSTRACT: Infrared spectra of the matrix isolated OMS, OM(η^2-SO), and OM(η^2-SO)(η^2-SO_2) (M = Ti, Zr, Hf) molecules were observed following laser-ablated metal atom reactions with SO_2 during condensation in solid argon and neon. The assignments for the major vibrational modes were confirmed by appropriate $S^{18}O_2$ and $^{34}SO_2$ isotopic shifts, and density functional vibrational frequency calculations (B3LYP and BPW91). Bonding in the initial OM(η^2-SO) reaction products and in the OM(η^2-SO)(η^2-SO_2) adduct molecules with unusual chiral structures is discussed.

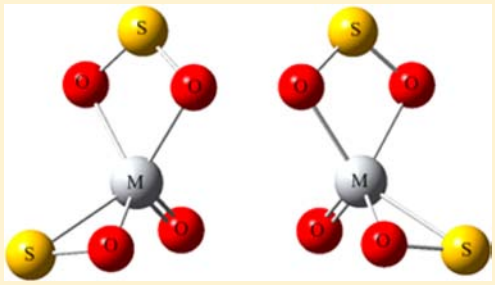

INTRODUCTION

Conversion of SO_2 to SO_3 is an important issue for the sulfuric acid industry. Recent study shows that oxidation of SO_2 to form SO_3 on vanadium oxide clusters reduces SO_2 to SO first, which then reacts with O_2 to give SO_3. Certain oxygen-rich metal oxide clusters provide one oxygen atom through an oxygen-detaching process followed by the reaction of O with SO_2 to give SO_3.[1,2] A systematic study on the adsorption and dissociation of SO_2 on different metal-based surfaces has been performed.[3−15] Both the pure metal (Zn, Mo, Mg, Sn)[12−15] and alkali or transition metal doped metal oxide surfaces[3−8,10,11] are higher in efficiency for S−O bond cleavage, while in contrast, the M_xO_y (M = Sc, Ti, V, Cr, Fe, Ni, Cu, Zn, Ce, Ba) surfaces are almost inactive instead.[3−8,10,11] Such observations combined with subsequent calculations confirm that effective S−O bond breaking only occurs in a proper electronic state on the target surface that is near the lowest unoccupied molecular orbital (LUMO) of SO_2; thus, the charge transfer between the metal surface and SO_2 plays vital role.

Coordination chemistry in and of sulfur dioxide have been investigated, and different bonding fashions of SO_2 coordination to transition metal center have been found.[16] Several transition metal cations and p-block metals coordinate SO_2 via oxygen to form η^1-O- complexes[16b,c] while for alkali metal−sulfur dioxide complexes O, O′-bridging SO_2 ligands have been characterized.[16a,d]

There has been extensive investigation of metal oxide molecules MO_x and oxygen complexes $M(O_2)_n$ by matrix infrared and electron spin resonance (ESR) spectroscopy;[17−24] however, mixed sulfur and oxygen analogues of these complexes have rarely been reported. Only recently laser-ablated uranium and group 6 metal atom reactions with SO_2 have been investigated,[25,26] which produced very stable SMO_2 (Cr, Mo, W, U) molecules that have been identified in neon and argon matrixes by infrared spectroscopy and reproduced by theoretical vibrational frequency calculations. Notice that SMO_2 molecules favor C_s structures for group 6 metals while the SUO_2 molecule is stabilized in a C_{2v} structure, which reflects the difference between d and f orbital participation in bonding and polarization of the outermost core shells.

In this paper we present a matrix infrared spectroscopic study of laser-ablated titanium, zirconium, and hafnium atom reaction products with SO_2 in solid argon and neon. The new metal sulfido oxides OM(η^2-SO) and its SO_2 adduct OM(η^2-SO)-(η^2-SO_2), and the simple sulfide-oxide OMS (M = Ti, Zr, Hf) are identified from matrix isolation infrared spectroscopy with isotopic substitution and theoretical vibrational frequency calculations.

EXPERIMENTAL AND COMPUTATIONAL METHODS

The experimental apparatus for investigating laser-ablated transition metal atom reactions with small molecules during condensation in excess argon or neon at 4 K has been described in our previous papers.[27,28] The Nd:YAG laser fundamental (1064 nm, 10 Hz repetition rate with 10 ns pulse width) was focused onto a rotating metal target, which gave a bright plume spreading uniformly to the cold CsI window. The titanium, zirconium, and hafnium targets (Alfa Aesar) were polished to remove oxide coating and immediately placed in the vacuum chamber. A mixture of $S^{18}O_2$ and $S^{16,18}O_2$ with a trace of $S^{16}O_2$ was prepared by tesla coil discharge of $^{18}O_2$ (>99%, SRICI) (about 2 Torr) in a 0.5 L pyrex bulb containing 10 mg of sulfur powder (99.5%, Alfa Aesar) sublimed onto the walls heated by external hot air (>450 °C). The sample of $^{34}SO_2$ was similarly prepared from sulfur-34 (98.8% ^{34}S, CIL) and oxygen (99.999%, BOC). The laser energy was varied about 10−20 mJ/pulse. FTIR spectra were recorded at 0.5 cm^{-1} resolution on a Bruker Vertex 80 V or Nicolet 750 instruments with 0.1 cm^{-1} accuracy using an MCTB detector. Matrix samples were annealed at different temperatures, and selected samples were subjected to photolysis by a medium pressure mercury arc lamp (Philips, 175W) with globe removed.

Received: May 3, 2012
Published: June 20, 2012

Table 1. Infrared Absorptions (cm^{-1}) Observed for Products of the Reaction of Ti, Zr, Hf Atoms and SO_2 Molecule

SO_2/Ar	$S^{18}O_2$/Ar	$^{34}SO_2$/Ar	SO_2/Ne	$S^{18}O_2$/Ne	$^{34}SO_2$/Ne	assignment
			Ti			
953.2	913.1	953.2	978.0		978.0	STiO
			987.4			SO_2^-
970.9	930.8	970.9	987.4	944.3	987.4	OTi(η^2-SO)
747.3	717.3	744.3	749.2	719.5	746.3	OTi(η^2-SO)
1008.6	966.8	1008.6	1015.8	985.6	1015.8	OTi(η^2-SO)(η^2-SO_2)
			973.5	939.6	965.4	OTi(η^2-SO)(η^2-SO_2)
			961.9	925.6	946.8	OTi(η^2-SO)(η^2-SO_2)
612.4	582.0	610.2	613.7	583.0	611.3	OTi(η^2-SO)(η^2-SO_2)
			536.1		536.3	OTi(η^2-SO)(η^2-SO_2)
			Zr			
877.4	835.1	877.4				SZrO
889.1	846.4	889.1	905.3	860.8	905.3	OZr(η^2-SO)
702.7	674.3	698.3	696.8		691.8	OZr(η^2-SO)
553.2	528.8		557.3		554.6	OZr(η^2-SO)
915.5	871.7	915.5	925.3	881.1	925.3	OZr(η^2-SO)(η^2-SO_2)
			978.4	943.8	968.8	OZr(η^2-SO)(η^2-SO_2)
			963.1	933.3	952.1	OZr(η^2-SO)(η^2-SO_2)
			886.1	852.8	878.0	OZr(η^2-SO)(η^2-SO_2)
586.2	561.7		591.6	563.5	587.5	OZr(η^2-SO)(η^2-SO_2)
			Hf			
876.9	831.4	876.9				SHfO
882.7	836.7	882.7	897.0	850.2	897.0	OHf(η^2-SO)
688.9	658.9	685.3	685.9	651.1	683.2	OHf(η^2-SO)
903.8	857.2	903.8	913.4	866.3	913.4	OHf(η^2-SO)(η^2-SO_2)
			973.5	938.2	960.3	OHf(η^2-SO)(η^2-SO_2)
			960.6	927.2	951.6	OHf(η^2-SO)(η^2-SO_2)
			875.7	841.2	869.7	OHf(η^2-SO)(η^2-SO_2)
607.4	563.3	602.8	608.0	577.2	605.3	OHf(η^2-SO)(η^2-SO_2)

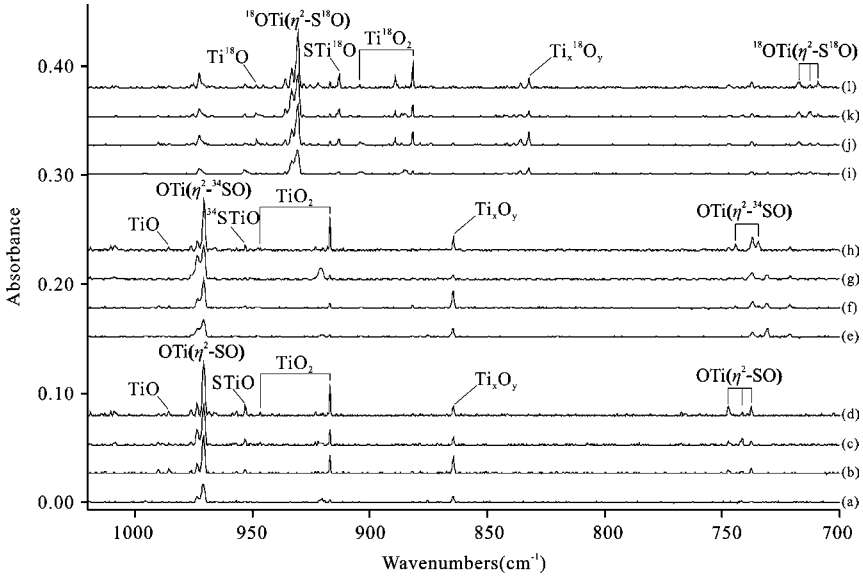

Figure 1. Infrared spectra for the titanium atom and SO_2 reaction products in solid argon at 4 K. (a) Ti + SO_2 deposition for 60 min; (b) after annealing to 20 K; (c) after >220 nm irradiation; (d) after annealing to 35 K; (e) Ti + $^{34}SO_2$ deposition for 60 min; (f) after annealing to20 K; (g) after >220 nm irradiation; (h) after annealing to 35 K; (i) Ti+ $S^{16,18}O_2$ deposition for 60 min; (j) after annealing to 20 K; (k) after >220 nm irradiation; (l) after annealing to 35 K.

Complementary density functional theory (DFT) calculations were performed using the Gaussian 03 program,[37] and the B3LYP functional, the 6-311++G(3df, 3pd) basis set for sulfur and oxygen atoms, and the SDD pseudo potential for titanium, zirconium, and hafnium[38−40] were employed. All of the geometrical parameters were fully optimized, and the harmonic vibrational frequencies were obtained analytically at the optimized structures.

RESULTS

Infrared spectra of laser ablated titanium, zirconium, and hafnium atom reaction products with SO_2 in excess argon or neon during condensation at 4 K will be presented in turn, and the new product absorptions are listed in Table 1. Density functional

dx.doi.org/10.1021/ic3008987 | Inorg. Chem. 2012, 51, 7415−7424

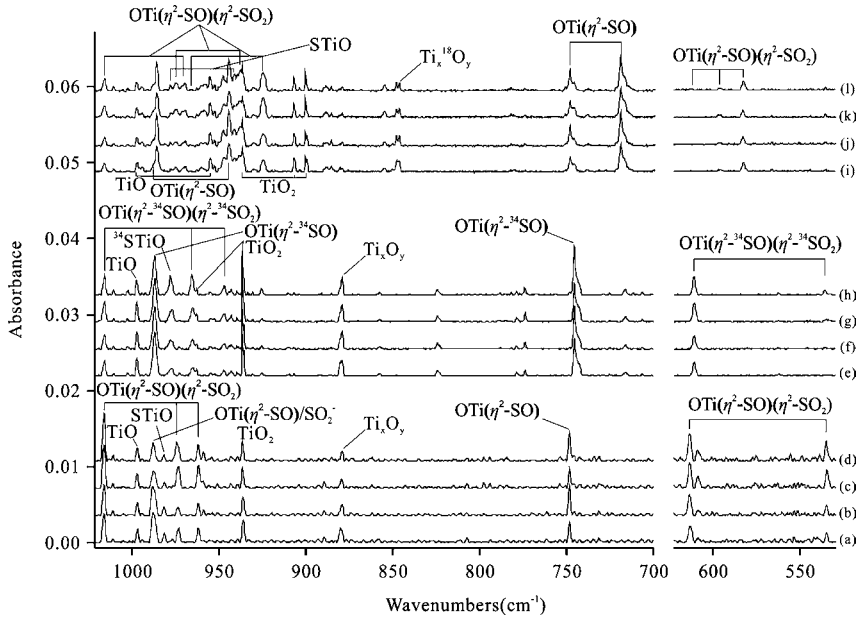

Figure 2. Infrared spectra for the titanium atom and SO_2 reaction products in solid neon at 4 K. (a) Ti + SO_2 deposition for 45 min; (b) after annealing to 8 K; (c) after >220 nm irradiation; (d) after annealing to 10 K; (e) Ti + $^{34}SO_2$ deposition for 45 min; (f) after annealing to 8 K; (g) after >220 nm irradiation; (h) after annealing to 10 K; (i) Ti + $S^{16,18}O_2$ deposition for 45 min; (j) after annealing to 8 K; (k) after >220 nm irradiation; (l) after annealing to 10 K.

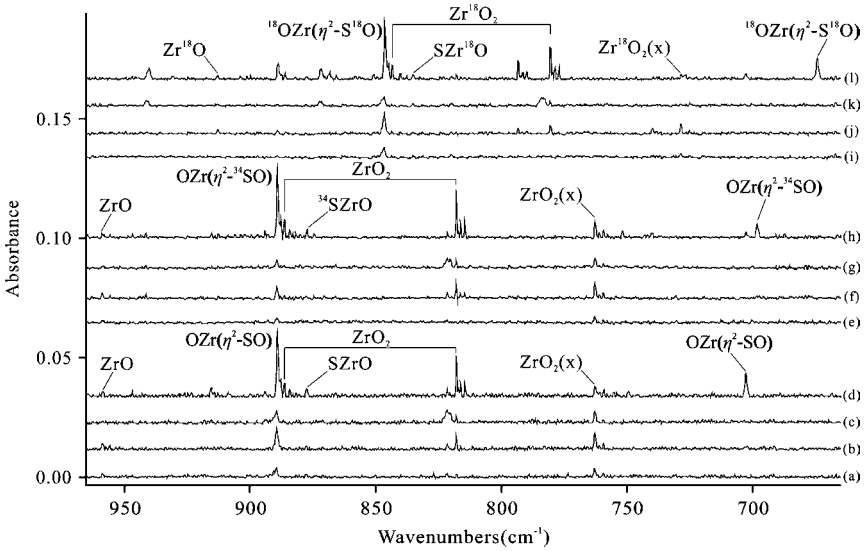

Figure 3. Infrared spectra for the zirconium atom and SO_2 reaction products in solid argon at 4 K. (a) Zr + SO_2 deposition for 60 min; (b) after annealing to 20 K; (c) after >220 nm irradiation; (d) after annealing to 35 K; (e) Zr + $^{34}SO_2$ deposition for 60 min; (f) after annealing to20 K; (g) after >220 nm irradiation; (h) after annealing to 35 K; (i) Zr + $S^{16,18}O_2$ deposition for 60 min; (j) after annealing to 20 K; (k) after >220 nm irradiation; (l) after annealing to 35 K.

calculations were performed to support the identification of new reaction products. Common species in these experiments, such as SO, SO_2^- and metal oxide absorptions, have been identified in previous papers.[17,24,29−31] Experiments were also done with $S^{18}O_2$ and $^{34}SO_2$, and the isotopic product frequencies are listed in Table 1.

Ti + SO_2. Infrared spectra of laser-ablated titanium atoms co-deposited with SO_2 in argon are shown in Figure 1. Strong bands at 970.9 cm^{-1} with matrix sites at 973.6 and 976.1 cm^{-1} and at 917.0 cm^{-1}, two medium intensity bands at 953.2, 864.5 cm^{-1}, and a weak band at 946.9 cm^{-1} were observed in the Ti═O stretching region after deposition. These bands increased on annealing to 20 K by 50% and broadened by full-arc irradiation, which, additionally, produced a new absorption at 1008.6 cm^{-1} in the same region. Further annealing to 35 K increased the 970.9, 953.2, 946.9, and 917.0 cm^{-1} bands dramatically. When neon was emloyed as a host matrix for similar reactions, new bands were observed at 987.4, 978.0, 936.5, and 879.3 cm^{-1} (Figure 2). Another three additional bands were observed at 1015.8, 973.5, and 961.9 cm^{-1} after deposition, which exhibited little changes on annealing, but increased markedly at the expense of band at 970.9 cm^{-1} on irradiation.

Zr + SO_2. Figure 3 shows laser ablated Zr atom reactions with SO_2 in excess argon. New absorptions were observed centered at 889.1 and 886.3 cm^{-1} in the Zr═O stretching region on deposition. These bands increased dramatically on annealing to 20 K, broadened

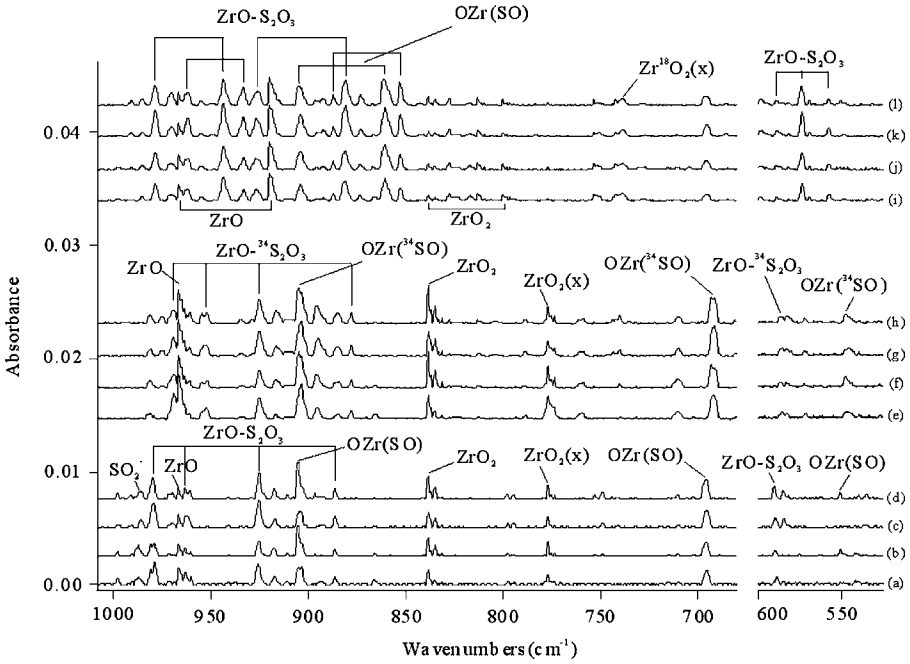

Figure 4. Infrared spectra for the zirconium atom and SO_2 reaction products in solid neon at 4 K. (a) Zr + SO_2 deposition for 45 min; (b) after annealing to 8 K; (c) after >220 nm irradiation; (d) after annealing to 10 K; (e) Zr + $^{34}SO_2$ deposition for 45 min; (f) after annealing to 8 K; (g) after >220 nm irradiation; (h) after annealing to 10 K; (i) Zr + $S^{16,18}O_2$ deposition for 45 min; (j) after annealing to 8 K; (k) after >220 nm irradiation; (l) after annealing to 10 K.

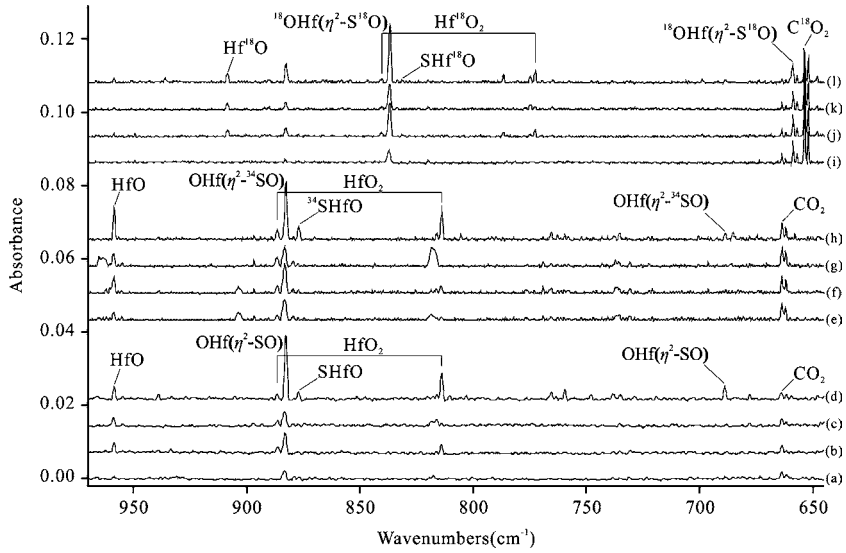

Figure 5. Infrared spectra for the hafnium atom and SO_2 reaction products in solid argon at 4 K. (a) Hf + SO_2 deposition for 60 min; (b) after annealing to 20 K; (c) after >220 nm irradiation; (d) after annealing to 35 K; (e) Hf + $^{34}SO_2$ deposition for 60 min; (f) after annealing to 20 K; (g) after >220 nm irradiation; (h) after annealing to 35 K; (i) Hf + $S^{16,18}O_2$ deposition for 60 min; (j) after annealing to 20 K; (k) after >220 nm irradiation; (l) after annealing to 35 K.

on full-arc irradiation, and further increased on annealing to 30 and 35 K. In addition, a photosensitive band at 915.5 cm^{-1} was also observed. Similar experiments in neon matrix are illustrated in Figure 4. Strong new bands at 978.4, 963.1, 925.3, 905.3, and 886.1 cm^{-1} appear on initial deposition and the sharp absorption at 905.3 cm^{-1} increased upon annealing and decreased on subsequent irradiation. These new absorptions are listed in Table 1.

Hf + SO_2. The reaction product spectra of hafnium with SO_2 in solid argon and neon are shown in Figures 5 and 6, and absorptions are listed in Table 1. One strong band at 882.7 cm^{-1} tracking with a weak peak at 688.9 cm^{-1} were the major product absorptions in solid argon, which appeared on deposition and increased markedly on annealing. New features were found at 973.5, 960.6, and 913.4 cm^{-1} in solid neon, which doubled on broadband irradiation but a 897.0 cm^{-1} band shows a substantial decrease (Figure 6).

Calculations. Figure 7 illustrates the structures calculated with B3LYP and BPW91 functionals for the insertion products OMS and OM(η^2-SO) (M = Ti, Zr, Hf), which were optimized to singlet ground states. The M═O and M−S bond lengths for OMS molecules increase while the OMS and OMO bond angles decrease from titanium to zirconium to hafnium. These

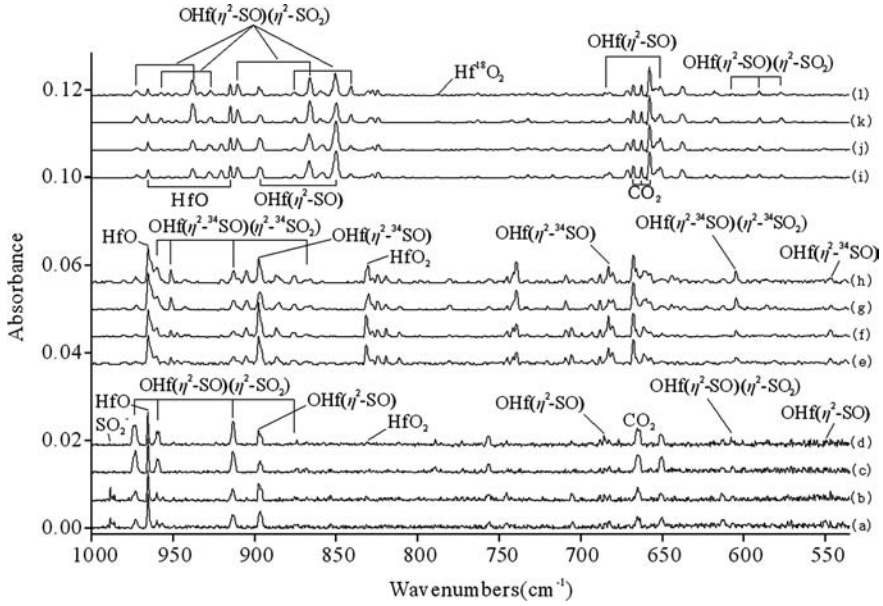

Figure 6. Infrared spectra for the hafnium atom and SO_2 reaction products in solid neon at 4 K. (a) Hf + SO_2 deposition for 45 min; (b) after annealing to 8 K; (c) after >220 nm irradiation; (d) after annealing to 10 K; (e) Hf + $^{34}SO_2$ deposition for 45 min; (f) after annealing to 8 K; (g) after >220 nm irradiation; (h) after annealing to 10 K; (i) Hf + S^{16},$^{18}O_2$ deposition for 45 min; (j) after annealing to 8 K; (k) after >220 nm irradiation; (l) after annealing to 10 K.

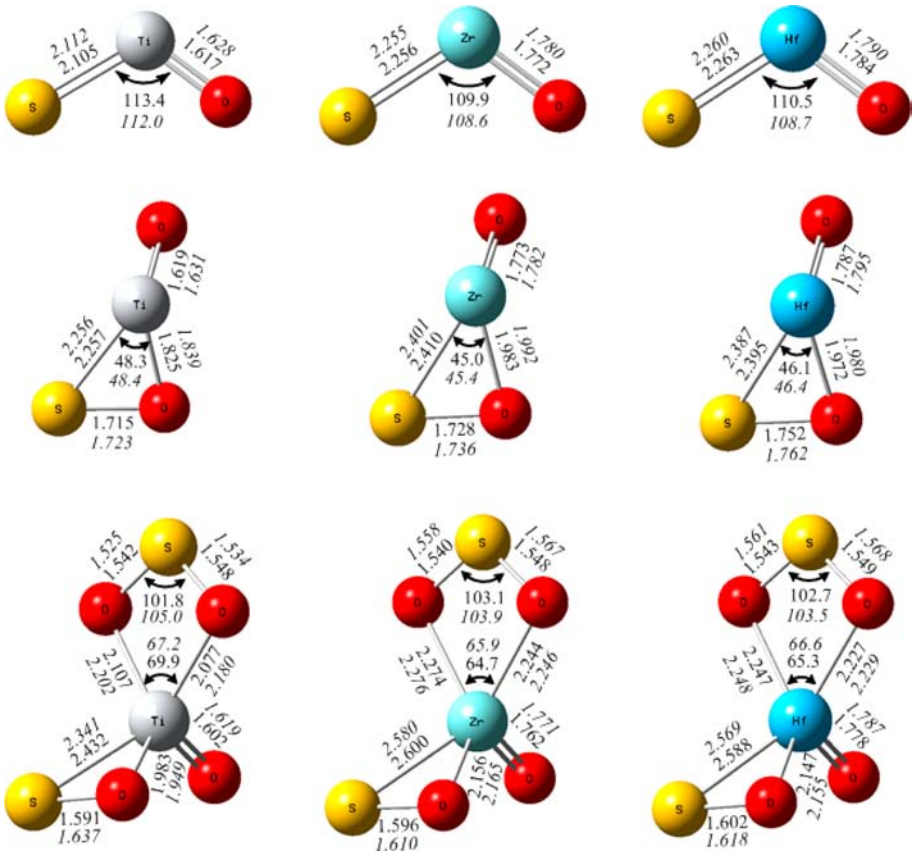

Figure 7. Optimized structures for SMO, OM(η^2-SO), and OM(η^2-SO)(η^2-SO_2) molecules based on B3LYP and BPW91 functional calculations (bond lengths in angstrom and bond angles in degree).

calculated structures are very similar to group 4 MO_3 molecules, but different pyramidal structures were observed in reactions of group 6 metal atoms with SO_2.[25,32] For the MO(η^2-SO) molecules the SO subunit is coordinated to MO, and the calculated trends of bond lengths and bond angles are the same as for the SMO molecules. One metal atom reaction with two SO_2 molecules gave the OM(η^2-SO)(η^2-SO_2) adducts, which were calculated to have triplet ground electronic states. Calculated frequencies for the OMS, OM(η^2-SO), and OM(η^2-SO)(η^2-SO_2) reaction products are listed in Tables 2−4, and natural

Table 2. Calculated Frequencies for OM(η^2-SO) (^{1}A) Isotopic Molecules (M = Ti, Zr, Hf)[a]

B3LYP			BPW91		
16-O	18-O	16-O/34-S	16-O	18-O	mode assignment
		OTi(η^2-SO)			
149.3(17.5)	144.5(16.2)	148.1(17.4)	140.4(15.4)	135.8(14.3)	S−Ti−O bend
237.5(30.9)	226.9(28.2)	237.5(30.9)	228.1(27.6)	217.9(25.1)	O−Ti−O bend
421.3(39.6)	418.9(38.7)	417.0(39.1)	416.7(34.7)	412.8(33.9)	Ti−SO str
582.3(14.2)	561.3(12.4)	578.2(14.4)	570.0(14.2)	549.6(12.7)	STiO def
770.8(108.1)	740.2(98.7)	767.8(108.2)	747.6(88.7)	718.0(80.8)	S−O str,
1040.9(338.1)	997.1(338.1)	1040.9(338.0)	1002.7(275.2)	960.5(258.7)	Ti═O str
		OZr(η^2-SO)			
139.6(15.8)	134.7(14.3)	138.4(15.8)	137.7(14.4)	132.7(13.0)	S−Zr−O bend
211.0(28.7)	200.6(26.0)	210.8(28.6)	207.0(24.1)	196.8(21.8)	O−Zr−O bend
375.7(35.4)	372.3(34.2)	368.3(34.5)	375.1(31.3)	371.8(30.2)	Zr−SO str
552.4(27.3)	529.4(25.3)	549.2(26.9)	539.4(24.5)	516.8(23.0)	SZrO def
708.2(95.8)	678.5(85.9)	704.0(96.3)	693.9(80.0)	665.1(71.5)	S−O str
920.9(260.7)	875.5(239.5)	920.1(259.8)	894.6(215.1)	850.6(197.6)	Zr═O str
		OHf(η^2-SO)			
140.2(15.9)	134.8(14.1)	139.2(16.0)	136.5(15.0)	131.0(13.4)	S−Hf−O bend
200.9(26.4)	190.7(23.7)	201.0(26.4)	200.2(21.4)	190.1(19.2)	O−Hf−O bend
358.5(30.0)	355.9(29.5)	351.3(29.1)	358.0(27.0)	355.5(26.5)	Hf−SO str
541.8(24.9)	519.7(22.1)	538.1(25.2)	527.7(20.8)	506.1(18.6)	SHfO def
682.5(86.9)	651.9(77.6)	679.7(87.5)	666.5(72.4)	636.9(64.5)	S−O str
888.8(193.9)	842.4(176.4)	889.1(194.4)	861.5(157.5)	816.6(143.2)	Hf═O str

[a]Frequencies and intensities (in parentheses) are in cm^{-1} and km mol^{-1}.

Table 3. Calculated Frequencies for OM(η^2-SO)(η^2-SO_2) (^{3}A) Isotopic Molecules (M = Ti, Zr, Hf)[a]

B3LYP			BPW91		
16-O	18-O	16-O/34-S	16-O	18-O	mode assignment
		OTi(η^2-SO)(η^2-SO_2)			
370.4(32.6)	360.0(29.0)	368.6(31.6)	373.6(14.2)	369.8(13.8)	Ti−SO str
535.1(112.4)	518.8(104.3)	534.6(108.8)	468.9(22.1)	451.0(20.3)	Ti−O str
612.1(171.0)	582.4(161.4)	610.3(176.8)	552.6(15.1)	528.4(14.1)	O═S═O bend
907.0(30.0)	872.3(28.7)	898.4(29.2)	816.0(165.3)	785.1(150.8)	S−O str
953.9(150.8)	918.9(138.9)	944.0(148.3)	924.2(90.2)	887.2(82.1)	S═O str
973.8(143.4)	937.5(135.9)	964.2(138.3)	1016.2(185.8)	973.6(176.8)	S═O str
1072.9(221.5)	1027.8(206.0)	1072.8(222.7)	1020.5(109.9)	984.5(99.7)	Ti═O str
		OZr(η^2-SO)(η^2-SO_2)			
327.5(26.4)	316.3(30.2)	325.9(23.4)	327.3(20.2)	316.4(21.0)	Zr−SO str
465.6(106.9)	445.6(104.5)	464.8(105.0)	451.0(85.8)	431.6(84.0)	Zr−O str
590.3(113.2)	560.7(97.4)	588.2(116.4)	559.4(94.9)	531.2(82.2)	O═S═O bend
896.2(36.2)	861.9(34.4)	887.6(35.2)	865.2(33.2)	832.1(32.8)	S−O str
939.4(247.3)	894.1(220.3)	936.7(245.1)	898.3(167.1)	859.9(169.3)	Zr═O str
956.6(138.1)	920.9(127.4)	948.2(142.7)	913.7(133.3)	874.6(96.8)	S═O str
977.0(140.1)	940.7(136.7)	967.4(130.9)	930.1(110.3)	895.8(110.7)	S═O str
		OHf(η^2-SO)(η^2-SO_2)			
325.9(5.3)	308.6(5.7)	325.9(5.3)	320.9(4.7)	304.1(5.3)	Hf−SO str
448.9(75.2)	426.5(71.7)	449.1(75.4)	431.8(57.4)	410.2(54.8)	Hf−O str
599.5(96.3)	569.2(81.6)	597.4(99.3)	567.2(77.0)	538.5(65.3)	O═S═O bend
885.0(41.1)	850.2(58.8)	876.6(37.5)	847.7(38.8)	813.5(52.7)	S−O str
905.8(178.4)	859.8(139.4)	905.9(183.6)	871.3(126.3)	828.2(95.1)	Hf═O str
955.2(150.5)	920.3(136.4)	945.2(148.9)	904.8(107.6)	871.0(97.1)	S═O str
970.4(141.1)	934.4(136.4)	960.8(134.2)	921.6(117.0)	888.1(113.8)	S═O str

[a]Frequencies and intensities (in parentheses) are in cm^{-1} and km mol^{-1}.

charge and Mulliken atomic spin densities for these molecules are given in Tables 5 and 6.

■ DISCUSSION

Infrared spectra of products formed in the reactions of laser ablated Ti, Zr, and Hf atoms with SO_2 in excess argon and neon during condensation at 4 K will be presented. Isotopic substitution and theoretical calculations were performed to support the identifications of new metal sulfide oxides.

MO(η^2-SO) (M = Ti, Zr, Hf). The laser-ablated Ti atom reaction with SO_2 in solid argon produced a stronger band at 970.9 cm^{-1} and a weaker band at 747.3 cm^{-1}, which show the

dx.doi.org/10.1021/ic3008987 | Inorg. Chem. 2012, 51, 7415−7424

Table 4. Calculated Frequencies of Isotopic SMO(^{1}A′) Molecules (M = Ti, Zr, Hf)[a]

B3LYP			BPW91		
16−32	18−32	16−34	16−32	18−32	mode assignment
		STiO			
247.4(6.5)	239.4(6.0)	245.6(6.3)	248.2(4.8)	240.1(4.4)	S═Ti═O bend
577.6(71.5)	577.2(70.2)	567.9(69.8)	559.9(58.7)	559.6(57.6)	Ti═S str
1034.5(308.0)	990.5(286.9)	1034.5(308.3)	999.1(246.2)	956.6(229.4)	Ti═O str
		SZrO			
219.9(5.8)	211.9(5.2)	218.3(5.8)	218.8(4.1)	210.9(3.6)	S═Zr═O bend
501.3(66.5)	500.3(65.7)	489.9(64.0)	493.2(54.8)	492.3(54.1)	Zr═S str
917.5(235.2)	872.3(214.2)	916.7(235.0)	893.4(191.8)	849.4(174.7)	Zr═O str
		SHfO			
206.6(6.9)	198.7(6.0)	205.4(6.9)	205.6(4.7)	198.0(4.0)	S═Hf═O bend
464.7(41.6)	465.0(41.5)	453.6(40.0)	459.3(34.6)	459.6(34.5)	Hf═S str
889.7(175.7)	843.4(158.5)	890.0(176.3)	863.8(139.8)	818.9(126.1)	Hf═O str

[a]Frequencies and intensities (in parentheses) are in cm^{-1} and km mol^{-1}.

Table 5. Natural Charge from NPA Analysis

molecule	atom	Ti	Zr	Hf	SO_2[c]
OM(η^2-SO) (^{1}A)	M[a]	1.49124	1.91799	2.04379	
	S	0.05813	−0.02200	−0.04032	1.62123
	O(M═O)[b]	−0.73346	−0.96166	−1.04265	−0.81062
	O(S−O)[b]	−0.81591	−0.93433	−0.96082	−0.81062

[a]:M represents corresponding metal atom in each column. [b]Represents corresponding atom in bracket. [c]NPA for SO_2 reactant.

Table 6. Mulliken Atomic Spin Densities for the ^{3}A OM(η^2-SO)(η^2-SO_2) Molecules

OM(η^2-SO)(η^2-SO_2)	atom	Ti	Zr	Hf
subunit: M	M	−0.037569	−0.002099	−0.006522
subunit: OM(η^2-SO)	O(M═O)[a]	0.024632	0.017472	0.027941
	S	0.746739	0.718337	0.711242
	O(S−O)[a]	0.282476	0.284760	0.288648
subunit: SO_2	S	0.677629	0.666074	0.670879
	O	0.162586	0.169409	0.160212
	O	0.162586	0.146047	0.147600

[a]Represents corresponding atom in bracket.

same behaviors on deposition, annealing, and irradiations, and therefore suggest that these two modes are due to the same molecule. With ^{18}O enriched sample these bands shifted to 930.8 and 717.3 cm^{-1} giving 1.0431 and 1.0418 ^{16}O/^{18}O isotopic frequency ratios. As shown in Figure 1 where there is about 10% SO_2 + 30% $S^{16,18}O_2$ + 60% $S^{18}O_2$) in the sample, two band, that is, doublet oxygen, isotopic distributions were observed for these two absorptions, which indicates the participation of one oxygen atom in each mode. With ^{34}S enriched sample (30% $^{32}SO_2$ and 70% $^{34}SO_2$), the 970.9 cm^{-1} band exhibits very little shift (to 970.7 cm^{-1}), suggesting very little S involvement in this vibration, while the 747.3 cm^{-1} band shifts to 744.3 cm^{-1} as appropriate for the S−O stretching mode. These two modes are characteristic of the OTi(η^2-SO) molecule.

In solid neon as shown in Figure 2, the Ti−O and S−O stretching modes for the OTi(η^2-SO) molecule are found at 987.4 and 749.0 cm^{-1}, respectively. These bands appeared on deposition, increased on annealing to 8 K, decreased after irradiation (>220 nm) but recovered on further annealing to 10 K in concert. Notice that the photosensitive band at 987.4 cm^{-1} is in agreement with the ν_1 fundamental of SO_2^- reported previously,[30] which overlaps with the Ti═O stretching mode of OTi(η^2-SO) in our experiment. Isotopic substituted precursors confirmed these assignments. With ^{18}O enriched samples, two bands shift to 944.3 and 719.5 cm^{-1} while in ^{34}S enriched samples, no shifts were observed for the Ti−O stretching mode but the S−O stretching mode shifted to 746.3 cm^{-1}.

In experiments for Zr reactions with SO_2 in argon (Figure 3), one strong absorption at 889.1 cm^{-1} in the Zr═O stretching region and a weak band at 702.7 cm^{-1} in the S−O stretching region track very well, which can be assigned to the OZr(η^2-SO) molecule. The 889.1 cm^{-1} band shows a 42.7 cm^{-1} $S^{18}O_2$ isotopic shift, but no shift with $^{34}SO_2$ sample. The ^{16}O/^{18}O isotopic frequency ratio 1.0504 suggests that this band is due to the Zr═O stretching vibration. The 702.7 cm^{-1} band exhibits a larger 28.4 cm^{-1} oxygen-18 shift and smaller 4.4 cm^{-1} sulfur-34 isotopic shift. The ^{16}O/^{18}O isotopic ratio 1.0421 and ^{32}S/^{34}S isotopic ratio 1.0063 indicate that this band is due to the S−O stretching vibration. The Zr═O and S−O stretching modes in solid neon were found at 905.3 and 696.8 cm^{-1}, respectively (Figure 4). In ^{18}O enrichment experiments, the former shifts to 860.8 cm^{-1} while the latter, unfortunately, is covered by absorptions due to CO_2. With the $^{34}SO_2$ sample the 905.3 cm^{-1} band shows no shift but the 696.8 cm^{-1} band shifts to 691.8 cm^{-1}.

In the case of hafnium (Figure 5), the strong band at 882.7 cm^{-1} is associated with the 688.9 cm^{-1} band on annealing and photolysis throughout our experiments, which can be assigned to the OHf(η^2-SO) molecule. Such assignment is further substantiated by observation of two fundamentals at 836.7 and 658.9 cm^{-1} in the ^{18}O enriched sample and at 897.0 and 685.3 cm^{-1} in the $^{34}SO_2$ sample. The ^{16}O/^{18}O isotopic ratios of 1.0550 and 1.0455 for both modes and ^{32}S/^{34}S isotopic ratio 1.0051 for the lower mode are very close to typical values for Hf═O and S−O stretching vibration modes. The behavior of the OHf(η^2-SO) molecule in excess neon is somewhat similar to that in solid argon (Figure 6). The absorptions due to the OHf(η^2-SO) molecule are identified as a Hf═O stretching mode

dx.doi.org/10.1021/ic3008987 | Inorg. Chem. 2012, 51, 7415−7424

at 897.0 cm^{-1} and a S−O stretching mode at 685.9 cm^{-1}. With $S^{16}O_2$/ $S^{18}O_2$ mixture, both modes are found in a doublet distribution which suggests only one oxygen atom participated in each vibration. With the ^{34}S enriched sample, the S−O stretching mode shows a red shift to 683.2 cm^{-1} giving the 1.0040 $^{32}S/^{34}S$ ratio, which is very close to the analogous mode ratios for OTi(η^2-SO) and OZr(η^2-SO).

DFT calculations support these assignments. With the B3LYP functional the Ti═O and S−O stretching modes for the OTi(η^2-SO) molecule are predicted at 1040.9 and 770.8 cm^{-1}, which are overestimated by 7.2% (Ar), 5.4%(Ne) and 3.1% (Ar), 2.8%(Ne), respectively. The predicted Ti═O stretching mode shows no shift while the S−O mode shifts red about 3.0 cm^{-1} upon ^{34}S substitution. With ^{18}O substitution the calculated Ti═O and S−O stretching modes give 1.0431(Ar), 1.0456(Ne) and 1.0418(Ar), 1.0413(Ne) $^{16}O/^{18}O$ isotopic frequency ratios, respectively, which match the observed values very well. When the BPW91 functional is used, these modes are calculated at 1002.7 and 747.6 cm^{-1}, which give very similar predictions. The Zr═O stretching frequency of OZr(η^2-SO) is calculated at 920.9 cm^{-1} (B3LYP) and 894.6 cm^{-1} (BPW91) with the S−O stretching mode at 708.2 cm^{-1} (B3LYP) and 693.9 cm^{-1} (BPW91). For all of above calculated frequencies, the maximum error is only 3.6%. Very similar frequency calculations were performed for OHf(η^2-SO) molecule, and as shown in Table 2, the calculations reproduced experimental values very well.

The insertion reactions of M (M = Ti, Zr, Hf) atoms into SO_2 to give OM(η^2-SO) are exothermic (ZPE correction included) by 112.0 kcal/mol (Ti), 139.5 kcal/mol (Zr), and 129.4 kcal/mol (Hf), respectively, based on B3LYP calculations.

$$M + SO_2 \rightarrow OM(\eta^2\text{-SO})$$

OMS (M = Ti, Zr, Hf). The strong band at 953.2 cm^{-1} in solid argon increased on annealing to 20 K after deposition (Figure 1), and annealing to 35 K doubled the absorbance for this band. The 953.2 cm^{-1} band shows no shift with $^{34}SO_2$ but shifts to 913.1 cm^{-1} with $S^{18}O_2$ sample, which is typical for a Ti═O stretching mode. This band appears lower than the TiO diatomic mode at 987.7 cm^{-1} but higher than the TiO_2 modes at 946.9 and 917.0 cm^{-1}. The triatomic OTiS molecule comes into mind for the 953.2 cm^{-1} band assignment. With the B3LYP functional TiO and TiS stretching modes of OTiS molecule were calculated at 1034.5 and 577.6 cm^{-1} (Table 4). However, the 577.6 cm^{-1} band is predicted to have only one-fifth the intensity of the 1034.5 cm^{-1} band, which suggests that this mode is too weak to be observed here. Analogous experiments were done in a neon matrix, and representative spectra are shown in Figure 2. A weak feature at 978.0 cm^{-1} is proper for Ti═O stretching mode of STiO, but the ^{18}O counterpart was not observed because of overlap by a very strong TiO_2 band at 936.5 cm^{-1}. Similar neon matrix shifts were observed for the stretching modes of TiO_2.[24]

Laser-ablated Zr atom reactions with SO_2 in argon produced a new Zr═O stretching frequency at 877.4 cm^{-1}, which was very weak on deposition and increased markedly on annealing to 35 K (Figure 3). This band shows no shift with enriched $^{34}SO_2$ sample, but shifts to 835.1 cm^{-1} with $S^{18}O_2$, giving the $^{16}O/^{18}O$ isotopic ratio 1.0507, which is appropriate for a Zr═O stretching mode of the OZrS molecule. A complementary experiment was performed using a neon matrix, but appropriate absorptions for OZrS were not observed. The Zr═O mode for OZrS in neon could locate around 903 cm^{-1} if we take a 25 cm^{-1} blue-shift from argon to neon for the OTiS molecule. However strong absorption at 905.3 cm^{-1} for OZr(η^2-SO) would cover this band.

The Hf═O stretching mode was found at 876.9 cm^{-1} for the OHfS molecule in solid argon (Figure 5), which is near the band at 877.4 cm^{-1} for OZrS, suggesting lanthanide contraction and relativistic effects for hafnium atom, as reported earlier for the dioxide molecules.[17] Diagnostic information from isotopic experiments further confirms the assignment; the Hf═O stretching mode was found at 831.4 cm^{-1} with $S^{18}O_2$, giving an isotopic $^{16}O/^{18}O$ ratio of 1.0547, but this mode exhibited no shift with $^{34}SO_2$. We did not observe the absorption of OHfS in solid neon, and the reasonable explanation could be made on the fact that absorptions due to Hf═O stretching mode for both OHf(η^2-SO) and OHfS are quite close with each other.

DFT frequency calculations support these OMS assignments. With the BPW91 functional the M═O stretching modes of the OMS molecules were calculated at 999.1 cm^{-1} (Ti), 893.4 cm^{-1} (Zr), and 863.8 cm^{-1} (Hf), which are overestimated by 4.8%, 1.8%, and −1.5%, respectively. The B3LYP functional gave slightly higher frequencies, but they are still in good agreement with group 4 metal oxide frequency calculations. Notice the predicted absorption of the M═S vibration is only 20%−25% of the M═O mode intensity for all three metals, and it was not observed in our experiments.

OM(η^2-SO)(η^2-SO_2) (M = Ti, Zr, Hf). As shown in Figure 4, new group of bands was observed at 978.4, 963.1, 925.3, 886.1, and 591.6 cm^{-1} in laser-ablated Zr atom reactions with SO_2 in solid neon where more diffusion takes place on sample deposition, and these bands are appropriate for the OZr(η^2-SO)(η^2-SO_2) adduct molecule. Irradiation (>220 nm) increased these bands 2-fold while the bands due to OZr(η^2-SO) at 905.3 and 696.8 cm^{-1} decreased by 50%, suggesting this enhancement comes at the expense of OZr(η^2-SO). In ^{18}O isotopic experiments the counterpart bands were found at 943.8, 933.3, 881.1, 852.8, and 563.5 cm^{-1} with $^{16}O/^{18}O$ isotopic ratios 1.0367, 1.0319, 1.0502, 1.0390, and 1.0499, respectively. Notice that the 925.3 cm^{-1} band shows the largest 1.0502 $^{16}O/^{18}O$ isotopic ratio, which is a typical heavy metal−oxygen stretching vibration mode, while the remaining bands with smaller $^{16}O/^{18}O$ isotopic ratios give evidence of sulfur−oxygen stretching and bending vibrations. The mixed $^{16}O/^{18}O$ sample (5% SO_2, 20% $S^{16,18}O_2$ and 75% $S^{18}O_2$) gave doublet oxygen isotopic distributions for the upper four bands along with triplet distribution for the bond at 563.5 cm^{-1} which indicates the involvement of one oxygen atom for each of the upper four modes and two oxygen atoms for 563.5 cm^{-1} band. With ^{34}S enriched sample, bands at 978.4, 963.1, 886.1, and 591.6 cm^{-1} shift to 968.8, 952.1, 878.0, and 587.5 cm^{-1}, giving 1.0099, 1.0116, 1.0092, and 1.0070 $^{32}S/^{34}S$ isotopic ratios, The 978.4 and 963.1 cm^{-1} bands can be assigned to S═O stretching modes while 886.1 and 591.6 cm^{-1} bands are due to the S−O stretching and O═S═O bending modes, respectively. The 925.3 cm^{-1} band shows no 34-S shift because of the Zr═O stretching mode barely perturbed by SO and SO_2 subunits. In solid argon very weak group bands at 966.9, 946.5, 915.4, and 877.2 cm^{-1} appeared on broadband irradiation and are due to the OZr(η^2-SO)(η^2-SO_2) molecule.

Our B3LYP functional calculation for OZr(η^2-SO)(η^2-SO_2) molecule gave a strong Zr═O stretching vibration at 939.4 cm^{-1}, two S═O stretching modes at 977.0 and 956.6 cm^{-1}, an S−O vibration at 896.2 cm^{-1} and an O═S═O bending mode at 590.3 cm^{-1}, which reproduced our observed values very well. The predicted $^{16}O/^{18}O$ isotopic ratios for Zr═O and S═O

stretching modes are essentially the same as our experimental values. The optimized structure for the OZr(η^2-SO)(η^2-SO_2) molecule with the ^{3}A ground state is very similar to OZr(η^2-O_2)(η^2-O_3) molecules obtained from reactions of Zr and O_2, for which the Zr═O stretching mode was observed at 912.9 cm^{-1} in solid argon.[33] This is very close to the same mode at 915.4 cm^{-1} for the OZr(η^2-SO)(η^2-SO_2) molecule in our argon matrix. Notice that the optimized structure shows two unequal S═O bond lengths: one is 0.01 Å longer than the other. The predicted isotopic 16,18-O distributions for the S═O stretching and O═S═O bending modes show doublet and triplet absorptions, respectively, suggesting that two S═O stretching modes vibrate separately while three atoms bends together. This calculated distribution is in excellent agreement with our experimental values. Notice that our OZr(η^2-SO)(η^2-SO_2) complex with η^2-O,O-coordination of SO_2 toward the metal center was stabilized (Figure 7). However two coordination modes, η^1-S and η^2-S,O, of SO_2 ligand to transition metal center were found in M(SO_2)$_2$(PPh_3)$_2$ (M = Ni, Pt) and Rh(NO)(SO_2)(PPh_3)$_2$ complexes[42] and η^1-O-coordination mode of SO_2 was characterized in transition metal cation complexes (e.g., [M(SO_2)$_x$-(AsF_6)$_2$] M = Mg, Mn, Fe, Co, Ni, Zn).[16]

In the hafnium atom reaction with SO_2 in solid neon (Figure 6), new bands at 973.5, 960.6, 913.4, 875.7, and 608.0 cm^{-1} were observed, which are due to the OHf(η^2-SO)(η^2-SO_2) molecule. The effect of 18-O and 34-S substitution on the spectra are very similar to the Zr case, so the assignment is straightforward. The 913.4 cm^{-1} band with the 1.0545 ^{16}O/^{18}O isotopic ratio is due to the Hf═O stretching mode while the 973.5 and 960.6 cm^{-1} bands are appropriate for S═O stretching, and the 608.0 cm^{-1} band should be assigned to an O═S═O bending mode.

Similar assignments are made for the OTi(η^2-SO)(η^2-SO_2) molecule as shown in Table 1 and Figure 2. Two S═O stretching modes appeared at 973.5 and 961.9 cm^{-1}, which are very close to the same modes observed for OZr(η^2-SO)(η^2-SO_2) and OHf(η^2-SO)(η^2-SO_2); however, the Ti═O stretching mode was observed higher at 1015.8 cm^{-1}. The S−O stretching mode was not observed because of band weakness. The 18-O and 34-S experiments gave similar isotopic shifts and distribution as shown in Figure 6.

The OM(η^2-SO)(η^2-SO_2) molecules can in principle be formed by adding SO_2 to OM(η^2-SO). Our B3LYP calculations predict the reactions to be exothermic by 45 kcal/mol (Ti), 51 kcal/mol (Zr), and 56 kcal/mol (Hf). Notice that the OM(η^2-SO)(η^2-SO_2) molecules are calculated to have triplet ground states, and their product yields were increased 2-fold by uv irradiation.

$$SO_2 + OM(\eta^2\text{-SO}) \xrightarrow{h\upsilon} OM(\eta^2\text{-SO})(\eta^2\text{-}SO_2)$$

Bonding. As has been discussed, insertion of M(Ti, Zr, Hf) into SO_2 to give the OM(η^2-SO) (^{1}A) molecule is a highly exothermic reaction, and the energy released is predicted to be 112(Ti), 140 (Zr), and 129 (Hf) kcal/mol. Reasons for the differences can be attributed to the core-like and less reactive nature of 3d orbitals.[17] NPA analysis summarized in Table 5 further confirm that charges centered on M and other atoms increase in series Ti−Zr−Hf, suggesting more electrons are participating in bonding and hence the more ionic bonds are formed. Bond component analysis for OM(η^2-SO) (^{1}A) based on NBO give an average d orbitals participation in bonding as 64.2% (Ti), 69.1% (Zr) and 64.4% (Hf). It is clear that d orbital participation increases from Ti to Zr and decreases from Zr to Hf, which is consistent with the reaction energy predicted and reflects the relativistic effects.[17,41]

For the complex OM(η^2-SO)(η^2-SO_2), DFT calculations indicate that all the three molecules are found in the triplet ground state, which are more stable than the corresponding singlet by energies of 22 (Ti), 23 (Zr), and 25 (Hf) kcal/mol. In addition, formation of the complex OM(η^2-SO)(η^2-SO_2) (^{3}A) is energetically preferred. Our calculated results suggest that once another SO_2 coordinates to OM(η^2-SO), the energy will be lowered by 45 to 56 kcal/mol from titanium to hafnium. However, the new adducts are all increased under λ > 220 nm irradiation as shown in Figures 4, 5, and 6. Noticing the ground state for SO_2 and OM(η^2-SO) are both singlet while that for OM(η^2-SO)(η^2-SO_2) is triplet. It seems reasonable that irradiations induced a charge transfer between two reactants leading to the reaction to proceed through an energy preferred channel. From Table 6, we also learn that the coordinated subunit SO along with SO_2 in OM(η^2-SO)(η^2-SO_2) (^{3}A) molecule are both found to concentrate spin densities. This distribution facilitates the activation of SO_2 and brings about two elongated S−O (1.54/1.55 Å) bonds as shown in Figure 7. The significant red-shift for the S═O stretching mode shows activation of the S═O bond through this molecule.

More interestingly, both OM(η^2-SO) and OM(η^2-SO)(η^2-SO_2) molecules exhibit chirality. Optimized molecules shown in Figure 8 are enantiomers with chiral metal centers. Origins for the formation of such molecules can be expected from the insertion reaction of M to SO_2 to produce different OM(η^2-SO) (^{1}A) molecules. Although the combination of quantum chemical calculations and vibrational absorption and circular dichroism spectra (VCD spectra) proved to be powerful in determining the absolute configuration of such molecules,[34] we cannot identify chiral molecules under our current experimental conditions. Since catalysts containing group 4 atoms have been applied extensively in enantioselective synthesis, asymmetric catalysis, and many other related areas,[35,36] the above mentioned mechanism for the formation of new adducts may be involved in one of the indispensible processes which are of prime importance to those areas.

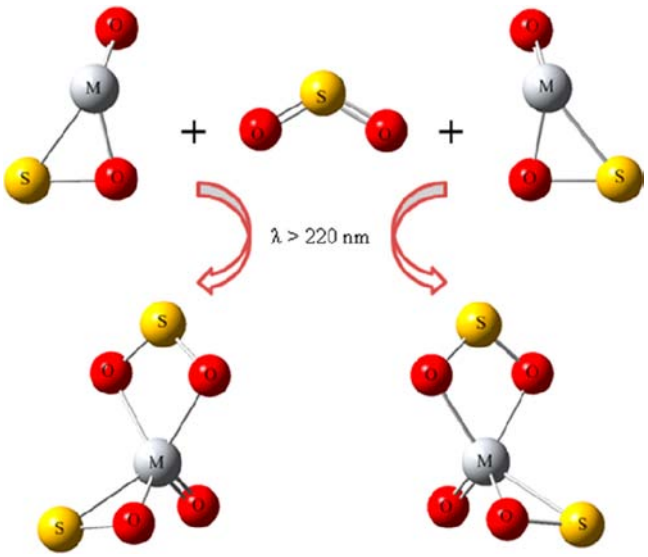

Figure 8. OM(η^2-SO) reaction with SO_2 (λ > 220 nm) giving OM(η^2-SO)(η^2-SO_2) with chiral molecules.

CONCLUSIONS

Laser-ablated group 4 atoms react with SO_2 during condensation in excess argon and neon at 4 K, and the new products are presented here. Infrared absorption bands for OMS and OM(η^2-SO) (M = Ti, Zr, Hf) are observed, and isotopic substitution and calculated frequencies of optimized structures further confirm the existence of these products. In the softer neon matrix new bands are assigned to adduct OM(η^2-SO)(η^2-SO_2) molecules. A bonding motif is also proposed for the OM(η^2-SO)(η^2-SO_2) molecules. More interestingly, optimized OM(η^2-SO) and OM(η^2-SO)(η^2-SO_2) molecules are enantiomers with chiral centers on M (Ti, Zr, Hf) which can find a meaningful role in enantioselective synthesis, asymmetric catalysis, and other related areas.

AUTHOR INFORMATION

Corresponding Author

*E-mail: xfwang@tongji.edu.cn (X.W.), lsa@virginia.edu (L.A.).

Notes

The authors declare no competing financial interest.

ACKNOWLEDGMENTS

We gratefully acknowledge financial support from NSFC Grant (20973126, 21173158) and STCSM Grant (10PJ1409600) to X.W, and DOE Grant DE-SC0001034 and NCSA computing Grant CHE07-0004N to L.A.

REFERENCES

(1) Jakubikova, E.; Bernstein, E. R. *J. Phys. Chem. A* **2007**, *111*, 13339.
(2) He, S. G.; Xie, Y.; Dong, F.; Heinbuch, S.; Jakubikova, E.; Rocca, J. J.; Bernstein, E. R. *J. Phys. Chem. A* **2008**, *112*, 11067.
(3) Zhao, X.; Hrbek, J.; Rodriguez, J. A.; Pe, M. *Surf. Sci.* **2006**, *600*, 229.
(4) Rodriguez, A.; Jirsak, T.; Hrbek, J. *J. Phys. Chem. B* **1999**, *103*, 1966.
(5) Rodriguez, J. A.; Jirsak, T.; González, L.; Evans, J.; Pérez, M. *J. Chem. Phys.* **2001**, *115*, 10914.
(6) Rodriguez, J. A.; Pérez, M.; Evans, J.; Liu, G.; Hrbek, J. *J. Chem. Phys.* **2005**, *122*, 241101.
(7) Rodriguez, J. a.; Jirsak, T.; Freitag, A.; Larese, J. Z.; Maiti, A. *J. Phys. Chem. B* **2000**, *104*, 7439.
(8) Rodriguez, A.; Liu, P.; Pe, M.; Liu, G.; Hrbek, J. *J. Phys. Chem. A* **2010**, *114*, 3802.
(9) Rodriguez, A.; Dvorak, J.; Jirsak, T. *J. Phys. Chem. B* **2000**, *104*, 11515.
(10) Schlereth, T. W.; Hedhili, M. N.; Yakshinskiy, B. V.; Gouder, T.; Madey, T. E. *J. Phys. Chem. B* **2005**, *109*, 20895.
(11) Rodriguez, A.; Liu, G.; Jirsak, T.; Hrbek, J.; Chang, Z.; Dvorak, J.; Maiti, A. *J. Am. Chem. Soc.* **2002**, *124*, 5242.
(12) Chaturvedi, S.; Rodriguez, A.; Jirsak, T.; Hrbek, J. *J. Phys. Chem. B* **1998**, *102*, 7033.
(13) Rodriguez, A.; Jirsak, T.; Chaturvedi, S.; Hrbek, J.; York, N. *J. Am. Chem. Soc.* **1998**, 11149.
(14) Rodriguez, J. A.; Ricart, J. M.; Clotet, A.; Illas, F. *J. Chem. Phys.* **2001**, *115*, 454.
(15) (a) Rodriguez, A.; Hrbek, J.; Jirsak, T. *Surf. Sci.* **1999**, *426*, 319. (b) Rodriguez, J. A.; Jirsak, T.; Chaturvedi, S.; Dvorak, J. *J. Mol. Catal. A: Chem* **2001**, *167*, 47.
(16) (a) Mews, R.; Lork, E.; Watson, P. E.; Gortler, B. *Coord. Chem. Rev.* **2000**, *197*, 277. (b) Akkuş, O. N.; Decken, A.; Knapp, C.; Passmore, J. *J. Chem. Crystallogr.* **2006**, *36*, 321−329. (c) Decken, A.; Knapp, C.; Nikiforov, G. B.; Passmore, J.; Rautiainen, J. M.; Wang, X.; Zeng, X. *Chem.−Eur. J.* **2009**, *15*, 6504. (d) Derendorf, J.; Kebler, M.; Knapp, C.; Ruhle, M.; Schulz, C. *Dalton Trans.* **2010**, *39*, 8671.
(17) Chertihin, G. V.; Andrews, L. *J. Phys. Chem.* **1995**, *99*, 6356.
(18) Chertihin, G. V.; Bare, W. D.; Andrews, L. *J. Phys. Chem. A* **1997**, *101*, 5090.
(19) Gong, Y.; Zhang, Q.; Zhou, M. *J. Phys. Chem. A* **2007**, *111*, 3534.
(20) Gong, Y.; Zhou, M. *J. Phys. Chem. A* **2008**, *112*, 9758.
(21) Gong, Y.; Zhou, M.; Tian, S. X.; Yang, J. *J. Phys. Chem. A* **2007**, *111*, 6127.
(22) Thompson, K. R.; Weltner, W. *J. Phys. Chem.* **1971**, *75*, 3243.
(23) Gong, Y.; Zhou, M. *J. Phys. Chem. A* **2007**, *111*, 8973.
(24) Gong, Y.; Zhou, M.; Andrews, L. *Chem. Rev.* **2009**, *109*, 6765.
(25) Wang, X.; Andrews, L.; Marsden, C. J. *Inorg. Chem.* **2009**, *48*, 6888.
(26) Wang, X.; Andrews, L.; Marsden, C. J. *J. Phys. Chem. A* **2009**, *113*, 8934.
(27) Andrews, L. *Chem. Soc. Rev.* **2004**, *33*, 123.
(28) Andrews, L.; Citra, A. *Chem. Rev.* **2002**, *102*, 885.
(29) Lo, W. J.; Wu, Y. J.; Lee, Y. P. *J. Chem. Phys.* **2002**, *117*, 6655.
(30) Forney, D.; Kellogg, C. B.; Thompson, W. E.; Jacox, M. E. *J. Chem. Phys.* **2000**, *113*, 86.
(31) Chen, L. S.; Lee, C. I.; Lee, Y. P. *J. Chem. Phys.* **1996**, *105*, 9454.
(32) Wang, X.; Andrews, L. *J. Phys. Chem. A* **2009**, *113*, 8934.
(33) Chertihin, G. V.; Andrews, L. *J. Phys. Chem.* **1995**, *99*, 6356.
(34) Martin, P. R.; Forsythe, I. D. *J. Phys. Chem.* **1994**, *98*, 11623.
(35) Wood, M. C.; Leitch, D. C.; Yeung, C. S.; Kozak, J. a.; Schafer, L. L. *Angew. Chem., Int. Ed.* **2007**, *46*, 354.
(36) Brunel, J. M.; Holmes, I. P. *Angew. Chem., Int. Ed.* **2004**, *43*, 2752.
(37) (a) Becke, A. D. *J. Chem. Phys.* **1993**, *98*, 5648. (b) Lee, C.; Yang, Y.; Parr, R. G. *Phys. Rev. B* **1988**, *37*, 785.
(38) Frisch, M. J.; Pople, J. A.; Binkley, J. S. *J. Chem. Phys.* **1984**, *80*, 3265.
(39) Andrae, D.; Haeussermann, U.; Dolg, M.; Stoll, H.; Preuss, H. *Theor. Chim. Acta* **1990**, *77*, 123.
(40) (a) Becke, A. D. *Phys. Rev. A* **1988**, *38*, 3098. (b) Perdew, J. P.; Burke, K.; Wang, Y. *Phys. Rev. B* **1996**, *54*, 16533 , and references therein. (c) See also: Becke, A. D. *J. Chem. Phys.* **1997**, *107*, 8554.
(41) Pyykko, P. *Chem. Rev.* **2012**, *112*, 371−384.
(42) (a) Kubas, G. J. *Inorg. Chem.* **1979**, *18*, 182. (b) Ryan, R. R.; Kubas, G. J.; Moody, D. C.; Eller, P. G. *Struct. Bonding (Berlin)* **1981**, *46*, 47.